Construction and Building Materials 290 (2021) 123206

Contents lists available at ScienceDirect

Construction and Building Materials

journal homepage: www.elsevier.com/locate/conbuildmat

Energy density and fracture parameters of coated Scots pine

Poorya Karvan, Seyed Mohammad Javad Razavi, Filippo Berto, Chiara Bertolin *

Norwegian University of Science and Technology, Department of Mechanical and Industrial Engineering, Trondheim 7491 Norway

HIGHLIGHTS

- Mode I fracture properties of Scots pine was investigated.
- The impact of RH change was analyzed on coated pine samples.
- DSV in decrease parts of load was utilized to define an onset of damage.
- Damaged specimens had higher DSV decrease and lower fracture toughness.
- Crack length in damaged specimens was observed to propagate due to DSV decrease.

ARTICLE INFO

Article history:
Received 27 January 2021
Received in revised form 19 March 2021
Accepted 27 March 2021

Keywords:
Wood
Fracture toughness
Relative humidity
Surface coating
Acoustic emission
Finite element analysis
Scots pine
Energy density

ABSTRACT

An attempt was made to investigate the Michalski's proven fluctuation theory through the use of the fracture characteristic and the energy density – dynamic surface value – of Scots pine coated with Renaissance wax, paraloid, and tar. The slices were acclimatized in a climate chamber with an abrupt drop of relative humidity from 80% to 30% while being monitored by acoustic emission. During this period, macro-cracks were formed in the slices coated with the paraloid and tar while those coated with Renaissance wax were remained undamaged. Moreover, fracture tests along with the Finite Element Analysis (FEA) were utilized to calculate the critical values of the stress intensity factor. Furthermore, the alternative correlation, accounting for the effect of different specimens' length, introduced into the ASTM E833 standard resulting in agreeable values of fracture toughness as compared with the experimental data. Finally, the relation between the crack propagation and the fracture toughness with the ductile (load increase) and the brittle (load decrease) portions of the dynamic surface value (DSV) was investigated. It was observed that the impact of the latter portion in the crack propagation of the undamaged slices was more dominant, while the portion contributed almost the same in crack propagation of the damaged slices.

1. Introduction

Renowned for its environmental benefits, wood has been a common material to use in construction. As a result of changes in the equilibrium relative humidity (ERH) during its lifetime, wood experiences variations in its water content causing the release of strain energy and consequently creation of micro-cracks. To prevent the damage, it is vital to monitor the cracking state at micro level for an early and accurate prediction of macro cracking by the use of Non-Destructive Techniques (NDT) methods, such as Acoustic Emission (AE) technique, the use of which is widely reported in the literature when a mechanical loading is present [1–10].

Berg and Gradin [11] employed the AE method to study the dependency of laterally and longitudinally compressed wood to temperature, moisture content, strain and loading direction, reporting that an increase in temperature resulted in reductions of modulus of elasticity, compression strength and the cumulated number of AE events. Reiterer et al. [12] investigated the ductility of softwoods and hardwoods subjected to the splitting test while monitoring the amplitude, frequency spectra, and cumulative AE counts. They showed the AE counts, to reach the maximum force for softwoods, is considerably higher than those of hardwoods, concluding that the formation of a process zone in the former comprises more micro-cracks compared to the latter. An investigation by Landis and Whittaker [13] showed a good agreement between the energy released by mode I crack propagation and the resulting detected AE energy in wood. Through analyzing the AE features, Ando et al. [14] suggested that due to the strength characteristics of old and new woods, it is feasible to reuse old woods in construction. Chen et al. [15] performed AE monitoring on specimens of hardwood and softwood subjected to static and fatigue torsional

* Corresponding author.
E-mail address: chiara.bertolin@ntnu.no (C. Bertolin).

https://doi.org/10.1016/j.conbuildmat.2021.123206
0950-0618/

Nomenclature:

A_f	fractured area
A_W	normalized third degree polynomial function of crack length
E_{AE}	acoustic emission energy
F_C	critical load
F_i	experimental Load
K_{IC}	theoretical critical stress intensity factor
K_Q	provisional critical stress intensity factor
$K_{I,i}$	stress intensity facture
$K_{IC,i}$	critical stress intensity factor
a_W	normalized crack length
$2H$	width of the specimen
DSV	dynamic surface value – energy density
RH	relative humidity
T	temperature
B	thickness of the specimen
a	crack length
t	specimen thickness
W	distance between the point of applied force and the end of the specimen
W_1	total length of the specimen

loading. While microcracks were observed on both softwoods and hardwood during the static torsional test, the number of AE counts in the latter was higher than the former. Moreover, in the torsional fatigue test, the total number of AE counts was reported to be higher than those in the static test. The AE was utilized by Ohuchi et al. [16] to investigate the value of fracture toughness for compact tension (CT) specimens at various crack systems and loading directions. It was reported a promising result for the use of the acoustic emission technique for the fracture process of the Tangential-Radial (TR) specimen. Dourado and Moura [17] studied the impact of temperature on the Mode I fracture toughness of *Pinus pinaster* Ait. In their study, the fracture tests were conducted on DCB specimens while the temperature was varied between 30 °C and 110 °C. It was observed that fracture properties of the wood deteriorated over the 90 °C.

The use of AE technique has been prevalent among researchers for ex-situ tests [18–22] while the utilization of this technique for the in-situ health monitoring campaigns is scarce in literature [23–27]. This study, therefore, aims to employ the AE technique on Scots pine samples while their surfaces are coated with Renaissance wax, paraloid, and tar and investigate the influence of a sharp drop of 50% in the value of relative humidity on their microcrack formations. Subsequent fracture toughness tests have been performed to analyze the proven fluctuation concept introduced by Michalski [28] in 1993. According to Pollack [29], the majority of released elastic energy for a ductile material is associated with the plastic deformation and formation of the crack, whereas for a brittle material, it contributes to acoustic emission and crack propagation. Hence, the term dynamic strain energy value (DSV) has been further investigated here to explain the relashionship between the energy released by the samples during the increase and decrease portions of the applied load and their influence on crack propagation. Finally, a third degree polynomial equation to calculate the fracture toughness was introduced by normalizing the crack length by the length of the tested (DCB) specimens. The fracture toughness values have been obtained using FEA. The findings of this study are beneficial and aligned with the ongoing research within the "Symbol - Sustainable Management of heritage Buildings in a Long-term perspective" project (2018–2021), coordinated by the Norwegian University of Science and Technology (NTNU).

2. Materials and method

2.1. Materials and testing condition

Three slices of Scots pine and two slices of Oak (not considered in this work) have been acclimatized in an HPP-IPPplus climate chamber (Memmert, Germany) at a constant RH of 80% and temperature of 20.5 °C for a period of 18 days from 20/05/2019 to 07/06/2019, while being monitored by the AE. Following the radial surface treatment of the slices by (i) Renaissance microcrystalline wax, (ii) 40% (w/v) solution of Paraloid B72 (Phase) in acetone (Sigma-Aldrich, 99.9%)–CS + P40– and (iii) tar coatings at the constant temperature of 20.5 °C, they were then subjected to an abrupt drop of RH to 30% and kept constant at this new environmental condition for the subsequent period 07/06/2019–28/06/2019. At the same time, a fourth slice, without coating, was kept at 50% RH for standard reference purposes (see Fig. 1).

From the four slices (i.e. 3 treated + 1 standard reference), a total of 11 specimens were produced, among which 3 specimens were disregarded due to the abnormal data recorded during the AE monitoring. Typical geometry of a DCB specimen is shown in Fig. 2. The geometry of the specimens in this study, however, varies from the standard values [30], mainly due to the choice - during their preparation - of maximizing their length in respect to the dimension of the wooden log from which they came. A summary of the geometry and notation of the specimens are listed in Table 1.

Fracture tests were conducted on the specimens using a universal testing machine-UTM (MTS producer), securing the samples utilizing specially created grippers with a constant displacement rate of 1.5 mm/min. Synchronized with the UTM, an F504B Stingray digital camera with a rate of 5 frames/s was used to analyse the crack length values. A thorough account of the experimental procedure is provided in ref. [31].

The three simultaneous techniques allowed to detect the energy released by the fracture over the fractured area, defined in [32] as Dynamic Surface Energy Value (DSV) defined as:

$$DSV^i = \frac{\Sigma \Delta E_{AE}}{\Sigma A_f} \tag{1}$$

Where $\Sigma \Delta E_{AE}$ is the sum of detected AE energy during load increase or decrease time only, and ΣA_f is the fractured area obtained by multiplying the crack length detected by the digital camera during these temporal ranges with the thickness of the sample. DSV is the fracture energy density and its meaning is further investigated in relation to the fracture toughness in the following sections.

Eventhough the fracture resistancec is generally regarded as a geometry independent characteristic of a material, it has been shown in the literature [33–35] that fracture resistance is impacted through variation of geometrical constraints in specific specimen geometries. Here, the value of fracture toughness (K_{IC}) was calculated through the modifications to the standard formula used for the DCB samples here reported in equation (2) [36]. In fact, the pine slices in this study underwent changes in the relative humidity in the climate chamber, and - as a result - they embedded micro-cracks creating a challenging task to produce specimens with lengths equal to the conventional CT geometry. To account

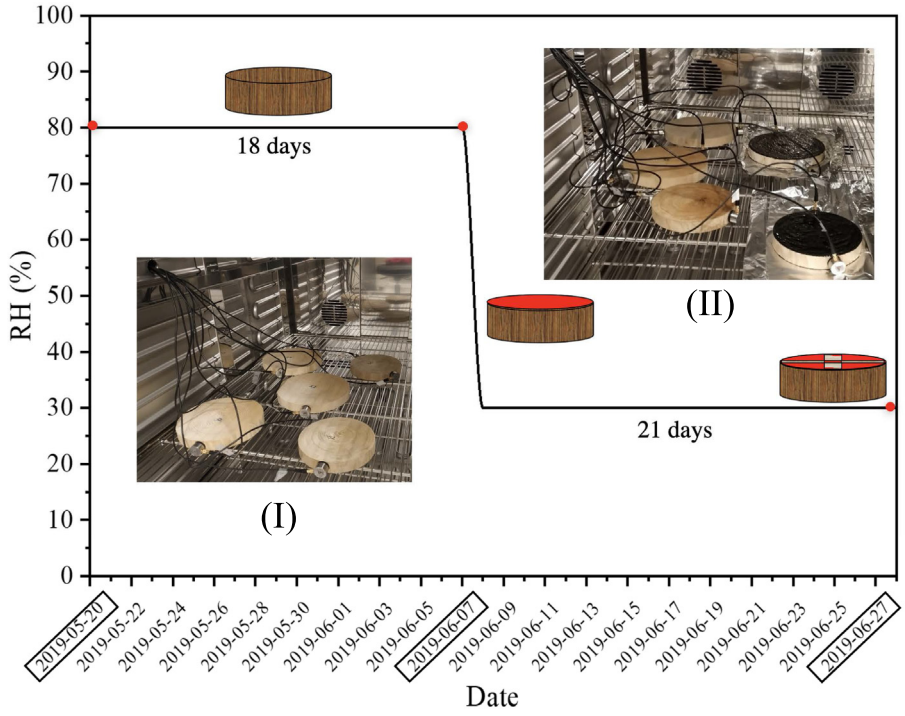

Fig. 1. Pine Slices tested in the climate chamber (I) before and (II) after the applied RH change with the coating treatment visible.

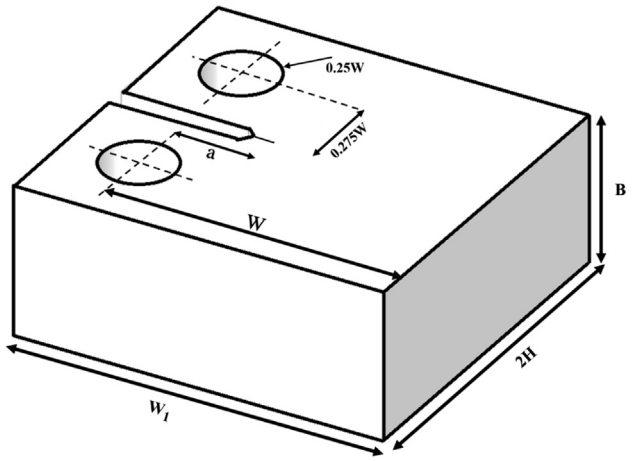

Fig. 2. Geometry of DCB specimen for fracture test (a = 10 mm).

for this variation, therefore, the values of the crack propagations were normalized by means of their respected length, providing a correlation, less dependent on the length of the specimens as:

$$K_{IC} = K_Q = \frac{F_C}{B\sqrt{W}} \cdot \frac{2 + A_W}{(1 - A_W)^{3/2}} \cdot \left[0,886 + 4,64(A_W) - 13,32(A_W)^2 + 14,72(A_W)^3 - 5,60(A_W)^4\right] \quad (2)$$

where K_Q is obtained from graphical construction of the load–displacement test record, term F_C is the critical force (i.e. the maximum force in each step of crack propagation), B and W are geometrical parameters as expressed in Fig. 2. Fig. 3 describes the new normalized crack propagation, A_W, defined as a third-degree polynomial function of the original normalized crack propagation, a_W, as:

$$A_w = 0.3421{a_W}^3 - 0.1588{a_W}^2 + 0.4637a_W + 0.3586 \quad (3)$$

2.2. Numerical analysis of fracture toughness

A 2D model was created in the Abaqus CAE 2019 [37] software to calculate the value of stress intensity factor, K_I measured at the crack tip in the significant points. 8-node plane strain elements were used to discretize the finite element model. To improve the accuracy of the results, a higher mesh density was employed in the proximity of the crack tip (see Fig. 4). Singular collapsed elements were integrated in the first ring around the crack tip to pre-

Table 1
Specimen coating and geometry as referred to Fig. 2.

Coating	Specimen ID	W_1 (mm)	a/W	2H (mm)	B (mm)
Wax	SP1.2	64.2	0.79	35.5	24.6
	SP1.3	81.3	0.86	35.5	19.7
	SP1.4	50.5	0.76	35.5	19.7
CS + P40	SP2.2	50	0.68	35.5	20.2
Tar	SP3.1	63.2	0.75	35.3	20.8
	SP3.2	84	0.77	35.6	19.9
Standard(No coating)	STP1	69.7	0.82	36.8	22

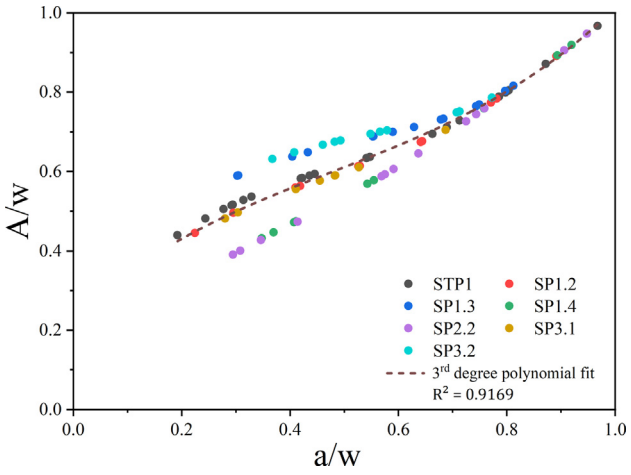

Fig. 3. Polynomial fit of the new normalized crack propagation (A_W) in respect the original normalized crack propagation (a_W).

cisely capture the stress singularity. In order to obtain the variation of stress intensity factor during the crack propagation, discrete steps of crack propagation were modeled with specific crack extension lengths corresponding to the progressive crack lengths during the fracture tests. Linear elastic analyses were performed using the material properties reported in [38]. The finite element models were loaded under unit concentrated force (i.e. 1 N) on the top loading hole while the boundary conditions were defined as shown in Figure. As the modelling outcome, the stress intensity factors, $K_{I,i}$ were obtained in each step of crack propagation. Using the values of stress intensity facture at specific crack lengths, $K_{I,i}$, and the corresponding experimental load, F_i, the fracture toughness, $K_{IC,i}$ was calculated as:

$$K_{IC,i} = K_{I,i} \cdot F_i \tag{4}$$

3. Results and discussion

In order to evaluate the capability of the modified equation, a comparison was made between the values of the fracture toughness obtained from the experimental approach ($K_{IC}^{(Exp)}$) with those calculated through equations (2) and (3), and the results are presented in Fig. 5. As shown in this figure, the calculated values of K_{IC} obtained by means of the modified correlation ($K_{IC}^{(Mod)}$ - black color) are in closer agreement with experimental values than those

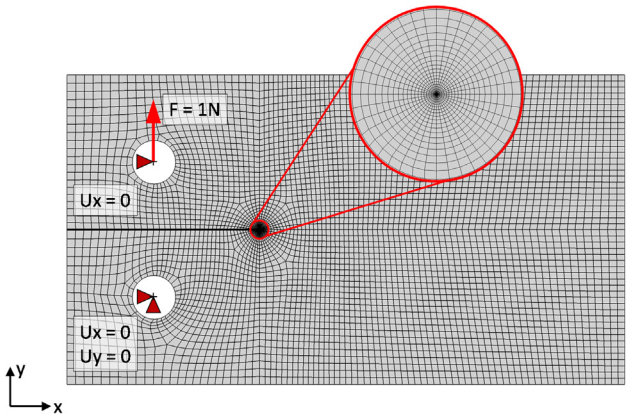

Fig. 4. Representative mesh pattern and applied boundary conditions in DCB model.

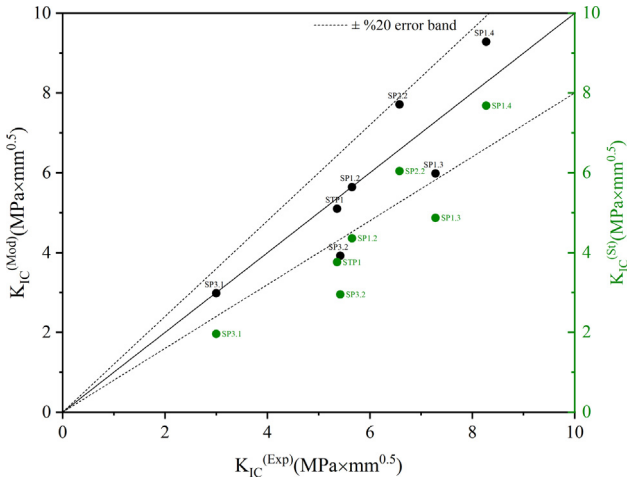

Fig. 5. Comparison between experimental $K_{IC}^{(Exp)}$ and calculated values of fracture toughness obtained by means of the standard ($K_{IC}^{(St)}$ - green dots) and modified ($K_{IC}^{(Mod)}$ - black dots) equations. Linear best fit (Continuous) and error band within ± 20% (Dotted black line). (For interpretation of the references to color in this figure legend, the reader is referred to the web version of this article.)

calculated through the standard correlation ($K_{IC}^{(St)}$ green color). While the mean value of error of the former approach is 3.12%, for the latter it is 25.91%, approximately one eight of the standard values.

As displayed in Fig. 6, only the pine slice with the renaissance microcrystalline wax coating (SP1) were remained intact at the conclusion of the test in the climate chamber, whereas those coated with CS + P40 (SP2) and Tar (SP3) experienced macro-cracking during the RH change. During the RH decrease, wood generally experiences shrinkage, due to water desorption, however, the coatings of the radial surfaces in SP2 and SP3, acted as constraints, preventing the desorption of water from the wood, and resulting in damaging the slices. While the coating in SP1 allowed water to desorb partially from the base surfaces and reduced the risk of macro-crack formation.

In order to quantitatively discriminate between the damaged and undamaged slices, the concept of DSV, dynamic surface energy

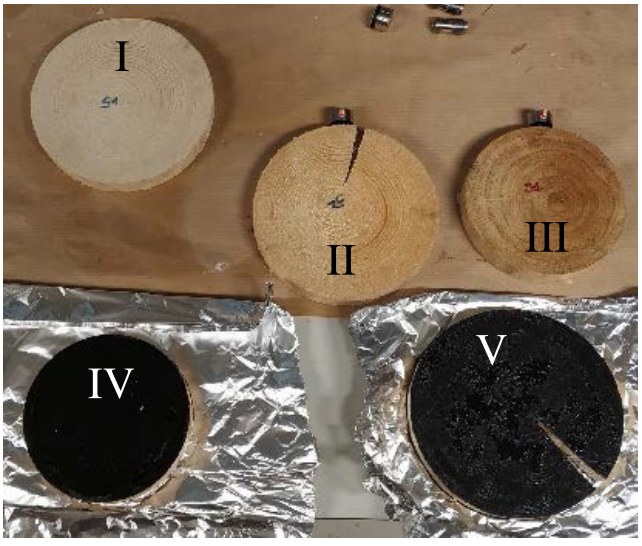

Fig. 6. (I) Pine coated with Renaissance microcrystalline wax, (II) pine coated with CS + P40, (III) Oak coated with CS + P40, (IV) oak coated with tar, and (V) pine coated with tar slices after the RH reduction.

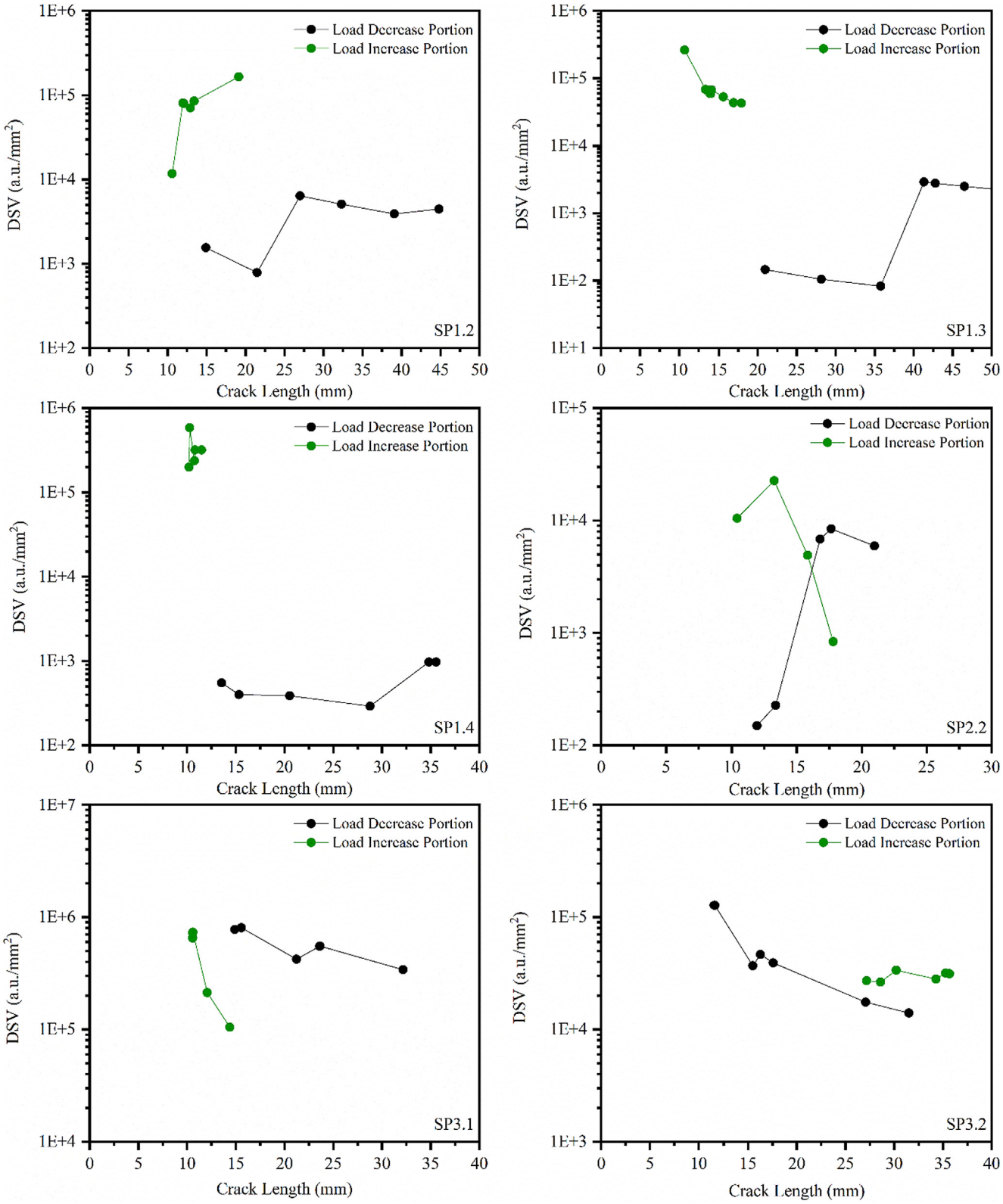

Fig. 7. The DSV vs. crack length for portions of load increase (green dots and lines) and decrease (black dots and lines) for the coated specimens while in climate chamber. Labels referring to the type of coating on the specimen are reported on the bottom right. (For interpretation of the references to color in this figure legend, the reader is referred to the web version of this article.)

value, as expressed in [32] and here reported in equation (1), was employed. The DSV was further categorized into those obtained during the load decrease and increase portions correspondingly associated with brittle and ductile fracture. To investigate the impact of the environmental modification in the climate chamber on the crack length of the slices, the values of DSV with respect to the crack length are presented in Fig. 7. The data recorded by the AE were classified into the portions of load decrease and

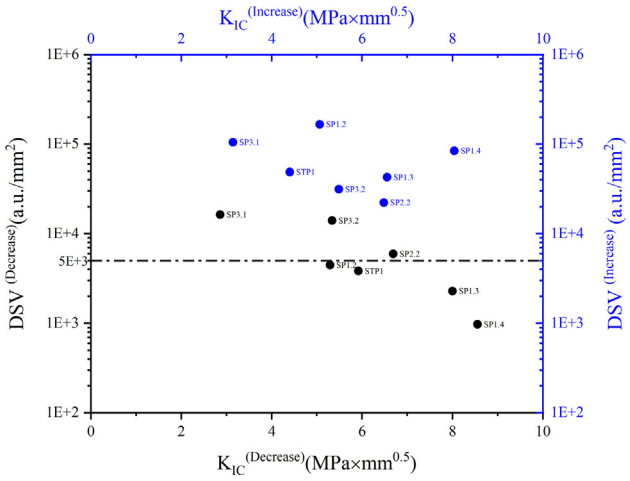

Fig. 8. Dynamic surface energy value vs fracture toughness for increments of load decrease and increase.

increase. There are two main points to be considered in this figure. First, is the values of DSV in the load increase and decrease parts and the values of the crack with respect to those loading parts. In this former context, the values of DSV for specimens SP1.2, SP1.3, and SP1.4 - with not macro-damaged after the test - differ vastly by an average scale of respectively 33, 100, and 300 between the load increase and load decrease parts, while this scale becomes almost equal for damaged specimens (i.e. SP2.2, SP3.1, SP3.2). Regarding the latter perspective, all specimens, apart from SP2.2, had almost comparable crack length for portions of load increase and decrease. This atypical behavior of the SP2.2 specimen can be attributed to the Paraloid coating.

Fig. 8 shows a compared visualization of the DSV amount in load increase and decrease portions drawn vs. their respected values of fracture toughness. The values of DSV differ vastly, with those related to load decrease (black color) considerably lower than those for load increase (blue color). The lower amount of DSV decrease corresponds to fractured samples coming from previously intact wood that was acclimatized with the surrounding environment without showing macro crack formation (i.e. SP1.x). Although not subjected to visual damage during the acclimatization test in the climate chamber, during the tensile tests, these samples demonstrated to be at higher risk as observed by larger crack propagation values reported in Table 2. While the higher amount of DSV decrease corresponds to fractured samples coming from previously damaged wood that during the acclimatization process in the chamber was subjected to complete plastic deformation resulting in final fracture. These tested samples are at lower risk when additional load is applied (e.g. during the tensile test) as the crack propagation is smaller. As indicated by the dashed line in this figure, in this study, an amount of 5000 DSV decrease was outlined as a threshold above which are the specimens belong to the latter group of specimen such as SP2.2, SP3.1, and SP3.2, while those below this line belong to the former. On the other hand, such distinction cannot be made with respect to the DSV increase values. This observation further elaborates on Pollock's report [29] that the ductile energy is released during the formation of the micro cracks, as opposed to brittle energy released in correspondence to the crack propagation and visible macro cracks.

The values of load increase and decrease parts, AE, crack length and lifetime for each sample are listed in Table 2. As shown in this table, the amount of AE and lifetime during the increase portion are considerably higher than the decrease one, however, the rate of energy release is significantly higher for the latter resulting in higher values of crack propagation as compared to the former.

According to Michalski's postulation of the proven fluctuation [28,39,40], an already cracked sample - when subjected to a relative humidity change - is less likely to damage further, as compared to an undamaged sample, when it undergoes the same or lower change widen in the relative humidity as occurred in its past. Although yet to be proven experimentally [41], this hypothesis is of utmost importance especially for the cultural heritage field, since the objects being dealt with have mostly undergone significant RH changes during their service life. Hence, defining a threshold in energy density, representing the maximum RH change to which a material was priorly subjected, is beneficial for making future maintenance and/or conservation scenarios. In this study, the intention was to investigate this postulation in more debt by: (1) clarifying the DSV or energy density – samples SP2.2, SP3.1, and SP3.2 are those with developed micro-cracks during the %50 RH change while having a DSV decrease of more than 5000, on other hand, the SP1.2, SP1.3, SP1.4 samples subjected to the relative humidity change fell below the threshold line of 5000 DSV decrease. According to Michalski's hypothesis, the former samples are safe if subjected to RH variations equal or less than %50, while the latter samples are prone to damage undergoing the same RH changes. (2) Understanding the relation between DSV and the fracture properties of the wood. The values of fracture toughness for the increasing portion are slightly higher for the cracked samples SP2.2, SP3.1, and SP3.2 as compared to uncracked samples of SP1. X and STP1 whose fracture toughness amounts are higher for the decreasing portion of the load. On the other hand, the more pronounced difference of DSV values between the load decrease and increase portions was observed for the latter group as opposed to the former group. Furthermore, even though this study has provided more insight into the proven fluctuation hypothesis by introducing a fracture characteristic (i.e. fracture toughness), there is still more research and analysis are needed in this field. Finally, analysis of the non-singular term of stress (T-stress) in calculations of the critical stress intensity factor, an in-depth investigation on a 3D FEA simulation of the DCB speciemen, and considering the effect of moisture content on fracture parameters are the subjects of onoing works of the authors.

Table 2
Values of AE, crack length, and lifetime for the increase and decrease increments of load.

Sample ID	A.E (a.u.)			Crack length (mm)			Lifetime ΔT (s)			AE/ΔT (1/s)		
	Increase	Decrease	Ratio (In/De)	Increase	Decrease	Ratio (In/De)	Increase	Decrease	Ratio (In/De)	Increase	Decrease	Ratio (In/De)
SP1.2	37,205,000.0	3,815,349.2	9.8	9.1	34.8	0.3	112,820.0	2,302.1	48.6	329.8	1,664.5	0.2
SP1.3	6,645,000.0	1,803,550.3	3.7	7.9	40.0	0.2	80,715.8	4,769.0	16.9	82.3	378.2	0.2
SP1.4	9,359,900.0	490,119.0	19.1	5.7	25.8	0.2	43,753.7	3,950.5	11.1	213.9	124.1	1.7
SP2.2	3,507,500.0	1,319,162.0	2.7	7.8	21.0	0.4	14,086.2	2,184.7	6.5	249.0	603.8	0.4
SP3.1	9,736,900.0	7,535,967.0	1.3	4.4	22.2	0.2	28,739.0	6,173.4	4.7	338.8	1,220.7	0.3
SP3.2	15,999,000.0	5,991,167.2	2.7	25.7	21.5	1.2	158,126.8	20,770.6	7.6	101.2	288.4	0.4
STP1	11,074,000.0	2,207,695.6	5.0	10.3	26.2	0.4	64,405.3	10,669.7	6.0	171.9	206.9	0.8

4. Conclusions

Prior to applying a sudden 50% drop in the relative humidity in a climate chamber in which they were kept for 22 days, slices of Scots pine were kept at 80% relative humidity for 18 days and were coated with Renaissance wax (slice 1), paraloid (slice 2), and tar (slice 3). While the former coated slice was remained uncracked at the end of the 40-day period, macro-cracks were initiated in the last two. The normalized 3rd degree polynomial function introduced in the fracture toughness calculation, to eliminate the effect of various lengths of the specimens and resulted in promising fracture toughness values as compared to those obtained experimentally. The analysis performed on the AE energy and the values of DSV during the ductile and brittle parts, together with values of fracture toughness and the crack length obtained from the FEA and experimental set up showed that the cracks in specimens cut from slice 1 were dominantly propagated due to the brittle portion of DSV, while the remaining specimens produced form the already damaged slices of 2 and 3 had cracks propagated due to an almost equal contribution of the brittle and the ductile portions. Based on the wood type and conditioning of them this study, a threshold for the DSV decrease was defined at 5000 a.u./mm^2 above which the slices were damaged. According to these findings and Michalski's proven fluctuation postulation, it was concluded that the specimens from slice 1 are more susceptible to damage with an applied relative humidity change of less than 50%, than those from slice 2 and slice 3.

CRediT authorship contribution statement

Poorya Karvan: Data curation, Formal analysis, Writing - original draft. **Seyed Mohammad Javad Razavi:** Software, Supervision, Validation, Writing - review & editing. **Filippo Berto:** Validation, Writing - review & editing. **Chiara Bertolin:** Conceptualization, Funding acquisition, Investigation, Methodology, Project administration, Resources, Supervision, Validation, Writing - review & editing.

Declaration of Competing Interest

The authors declare that they have no known competing financial interests or personal relationships that could have appeared to influence the work reported in this paper.

Acknowledgments

Chiara Bertolin is indebted to the technical staff of the Mechanical and Industrial Engineering (MTP) department of NTNU. Special thanks to Carl-Magnus Mitbø, Børge Holen, and the Post Doc Dr. Lavinia de Ferri, financed by SyMBoL, which helped in performing the climate chamber and the calibration tests conceived by the principal investigator and coordinator of the SyMBoL Project: Chiara Bertolin.

Funding Sources List

The theoretical study and the experimental activity have been possible thanks to the Norwegian Research Council funded by the "SyMBoL–Sustainable Management of Heritage Building in a Long-term Perspective" Project (project no. 274749).

References

[1] P. Rodríguez, T.B. Celestino, Application of acoustic emission monitoring and signal analysis to the qualitative and quantitative characterization of the fracturing process in rocks, Eng. Fract. Mech. 210 (2019) 54–69, https://doi.org/10.1016/j.engfracmech.2018.06.027.
[2] L.H. Chen, W.C. Chen, Y.C. Chen, Shear fracture evolution in rocks examined using a novel shear device associated with acoustic emissions, Eng. Fract. Mech. 210 (2019) 42–53, https://doi.org/10.1016/j.engfracmech.2018.07.003.
[3] S. Aicher, L. Hofflin, G. Dill-Langer, Damage evolution and acoustic emission of wood at tension perpendicular to fiber, Holz Als Roh - Und Werkst. 59 (1-2) (2001) 104–116, https://doi.org/10.1007/s001070050482.
[4] M.F.S.F. de Moura, J.M.Q. Oliveira, J.J.L. Morais, N. Dourado, Mixed-mode (I + II) fracture characterization of wood bonded joints, Constr. Build. Mater. 25 (4) (2011) 1956–1962, https://doi.org/10.1016/j.conbuildmat.2010.11.060.
[5] F. Lamy, M. Takarli, N. Angellier, F. Dubois, O. Pop, Acoustic emission technique for fracture analysis in wood materials, Int. J. Fract. 192 (1) (2015) 57–70, https://doi.org/10.1007/s10704-014-9985-x.
[6] N. Dourado, F.G.A. Silva, M.F.S.F. de Moura, Fracture behavior of wood-steel dowel joints under quasi-static loading, Constr. Build. Mater. 176 (2018) 14–23, https://doi.org/10.1016/j.conbuildmat.2018.04.230.
[7] A.P. Schniewind, S.L. Quarles, S.H. Lee, Wood fracture, acoustic emission, and the drying process Part 1. Acoustic emission associated with fracture, Wood Sci. Technol. 30 (1996) 273–281, https://doi.org/10.1007/BF00229350.
[8] C. Wu, N. Vahedi, A.P. Vassilopoulos, T. Keller, Mechanical properties of a balsa wood veneer structural sandwich core material, Constr. Build. Mater. 265 (2020) 120193, https://doi.org/10.1016/j.conbuildmat.2020.120193.
[9] R.Y. Vun, F.C. Beall, Monitoring creep-rupture in oriented Strandboard using acoustic emission: Effects of moisture contenta, Holzforschung 58 (2004) 387–399, https://doi.org/10.1515/HF.2004.059.
[10] M. Diakhate, N. Angellier, R. Moutou Pitti, F. Dubois, On the crack tip propagation monitoring within wood material: Cluster analysis of acoustic emission data compared with numerical modelling, Constr. Build. Mater. 156 (2017) 911–920, https://doi.org/10.1016/j.conbuildmat.2017.09.065.
[11] J.E. Berg, P.A. Gradin, Effect of temperature on fracture of spruce in compression, investigated by use of acoustic emission monitoring, J. Pulp Pap. Sci. 26 (2000) 294–299.
[12] A. Reiterer, S.E. Stanzl-Tschegg, E.K. Tschegg, Mode I fracture and acoustic emission of softwood and hardwood, Wood Sci. Technol. 34 (5) (2000) 417–430, https://doi.org/10.1007/s002260000056.
[13] E.N. Landis, D.B. Whittaker, Acoustic emissions and the fracture energy of wood, in: Proc. Sess. Eng. Mech. 2000 - Cond. Monit. Mater. Struct., 2000: pp. 21–29. https://doi.org/10.1061/40495(302)2.
[14] K. Ando, Y. Hirashima, M. Sugihara, S. Hirao, Y. Sasaki, Microscopic processes of shearing fracture of old wood, examined using the acoustic emission technique, J. Wood Sci. 52 (6) (2006) 483–489, https://doi.org/10.1007/s10086-005-0795-7.
[15] Z. Chen, B. Gabbitas, D. Hunt, Monitoring the fracture of wood in torsion using acoustic emission, J. Mater. Sci. 41 (12) (2006) 3645–3655, https://doi.org/10.1007/s10853-006-6292-6.
[16] T. Ohuchi, A. Hermawan, N. Fujimoto, Basic studies on fracture toughness of sugi and acoustic emission, J. Fac. Agric. Kyushu Univ. 56 (2011) 99–102.
[17] N. Dourado, M.F.S.F. de Moura, Effect of temperature on the fracture toughness of wood under mode I quasi-static loading, Constr. Build. Mater. 223 (2019) 863–869, https://doi.org/10.1016/j.conbuildmat.2019.07.036.
[18] M. Strojecki, C. Colla, M. Łukomski, E. Gabrielli, Kaiser effect in historic timber elementsKaiser-Effekt in historischen Holzbalken, Eur. J. Wood Wood Prod. 71 (6) (2013) 787–793, https://doi.org/10.1007/s00107-013-0738-8.
[19] F. Baensch, M.G.R. Sause, A.J. Brunner, P. Niemz, Damage evolution in wood - Pattern recognition based on acoustic emission (AE) frequency spectra, Holzforschung 69 (2015) 357–365, https://doi.org/10.1515/hf-2014-0072.
[20] S. Kawamoto, R.S. Williams, Acoustic emission and acousto-ultrasonic techniques for wood and wood-based composites, Gen. Tech. Rep. (2002) 1–16.
[21] W. Moliński, J. Raczkowski, L. Muszyński, Acoustic emission generated upon mechano-sorptive creep of wood bent across to the grain under asymmetrical moistening, Holzforschung 54 (2000). https://doi.org/10.1515/HF.2000.051
[22] P. Tukiainen, M. Hughes, The effect of temperature and moisture content on the fracture behaviour of spruce and birch, Holzforschung 70 (2016) 369–376, https://doi.org/10.1515/hf-2015-0017.
[23] M. Noguchi, R. Ishii, Y. Fujii, Y. Imamura, Acoustic emission monitoring during partial compression to detect early stages of decay, Wood Sci. Technol. 26 (1992) 279–287, https://doi.org/10.1007/BF00200163.
[24] P. Palma, R. Steiger, Structural health monitoring of timber structures – Review of available methods and case studies, Constr. Build. Mater. 248 (2020) 118528, https://doi.org/10.1016/j.conbuildmat.2020.118528.
[25] A. Carpinteri, G. Lacidogna, Structural monitoring and integrity assessment of medieval towers, J. Struct. Eng. 132 (11) (2006) 1681–1690, https://doi.org/10.1061/(ASCE)0733-9445(2006)132:11(1681).
[26] A. Carpinteri, G. Lacidogna, A. Manuello, G. Niccolini, A study on the structural stability of the Asinelli Tower in Bologna, Struct. Control Heal. Monit. 23 (4) (2016) 659–667, https://doi.org/10.1002/stc.v23.410.1002/stc.1804.
[27] A. Manuello Bertetto, D. Masera, A. Carpinteri, Acoustic emission monitoring of the turin cathedral bell tower: Foreshock and aftershock discrimination, Appl. Sci. 10 (11) (2020) 3931, https://doi.org/10.3390/app10113931.
[28] S. Michalski, Relative humidity: a discussion of correct/incorrect values, ICOM Comm. Conserv. 10th Trienn. Meet. Washington, DC, 22-27 August 1993 Prepr. II (1993) 624–629.
[29] A.A. Pollock, Material brittleness and the energetics of acoustic emission, in: Conf. Proc. Soc. Exp. Mech. Ser., Springer New York LLC, 2011: pp. 73–79. https://doi.org/10.1007/978-1-4419-9798-2_10.

[30] T.W.H. Wang, F.D. Blum, L.R. Dharani, Effect of interfacial mobility on flexural strength and fracture toughness of glass/epoxy laminates, J. Mater. Sci. 34 (1999), https://doi.org/10.1023/A:1004676214290.
[31] C. Bertolin, L. de Ferri, J. Razavi, F. Berto, Acoustic Emission NDT for monitoring hygro-mechanical reactions of coated pine wood: a methodological approach, Procedia Struct. Integr. 28 (2020) 208–217, https://doi.org/10.1016/j.prostr.2020.10.026.
[32] Chiara Bertolin, Lavinia de Ferri, Filippo Berto, Calibration method for monitoring hygro-mechanical reactions of pine and oak wood by acoustic emission nondestructive testing, Materials (Basel). 13 (17) (2020) 3775, https://doi.org/10.3390/ma13173775.
[33] M.R. Ayatollahi, S.M.J. Razavi, M. Rashidi Moghaddam, F. Berto, Mode I Fracture Analysis of Polymethylmetacrylate Using Modified Energy-Based Models, Phys. Mesomech. 18 (4) (2015) 326–336, https://doi.org/10.1134/S1029959915040050.
[34] M.R. Ayatollahi, M. Rashidi Moghaddam, S.M.J. Razavi, F. Berto, Geometry effects on fracture trajectory of PMMA samples under pure mode-I loading, Eng. Fract. Mech. 163 (2016) 449–461, https://doi.org/10.1016/j.engfracmech.2016.05.014.
[35] S.M.J. Razavi, M.R. Ayatollahi, F. Berto, A synthesis of geometry effect on brittle fracture, Eng. Fract. Mech. 187 (2018) 94–102, https://doi.org/10.1016/j.engfracmech.2017.10.022.
[36] Chiara Bertolin, Poorya Karvan, Andrea De Rosa, Seyed Mohammad Javad Razavi, Filippo Berto, Relation between fracture characteristics and moisture content along longitudinal direction in a naturally drying Scots pine, Theor. Appl. Fract. Mech. 112 (2021) 102911, https://doi.org/10.1016/j.tafmec.2021.102911.
[37] ABAQUS, Abaqus 6.19, Dassault Systèmes Simulia Corp., Provid. RI, USA. (2019).
[38] Forest Products Laboratory - USDA, Wood Handbook: Wood as an Engineering Material, USDA - Gen. Tech. Rep. General Te (2010) 508.
[39] S. Michalski, The Ideal Climate, Risk Management, the ASHRAE Chapter, Proofed Fluctuations, and Toward a Full Risk Analysis Model, Contrib. to Expert. Roundtable Sustain. Clim. Manag. Strateg. Held April 2007, Tenerife, Spain. (2007).
[40] S. Michalski, The power of history in the analysis of collection risks from climate fluctuations and light, ICOM-CC 17th Trienn. Conf. 2014 Melbourne, Prev. Conserv. (2014).
[41] M. Eibl, A. Burmester, Learning from history: historic indoor climate conditions and climate control strategies, in: Postprints Munich Clim. Conf. "Climate Collect. Stand. Uncertainties", 7-9 Novemb. 2012, 2013.